Supplementary Materials

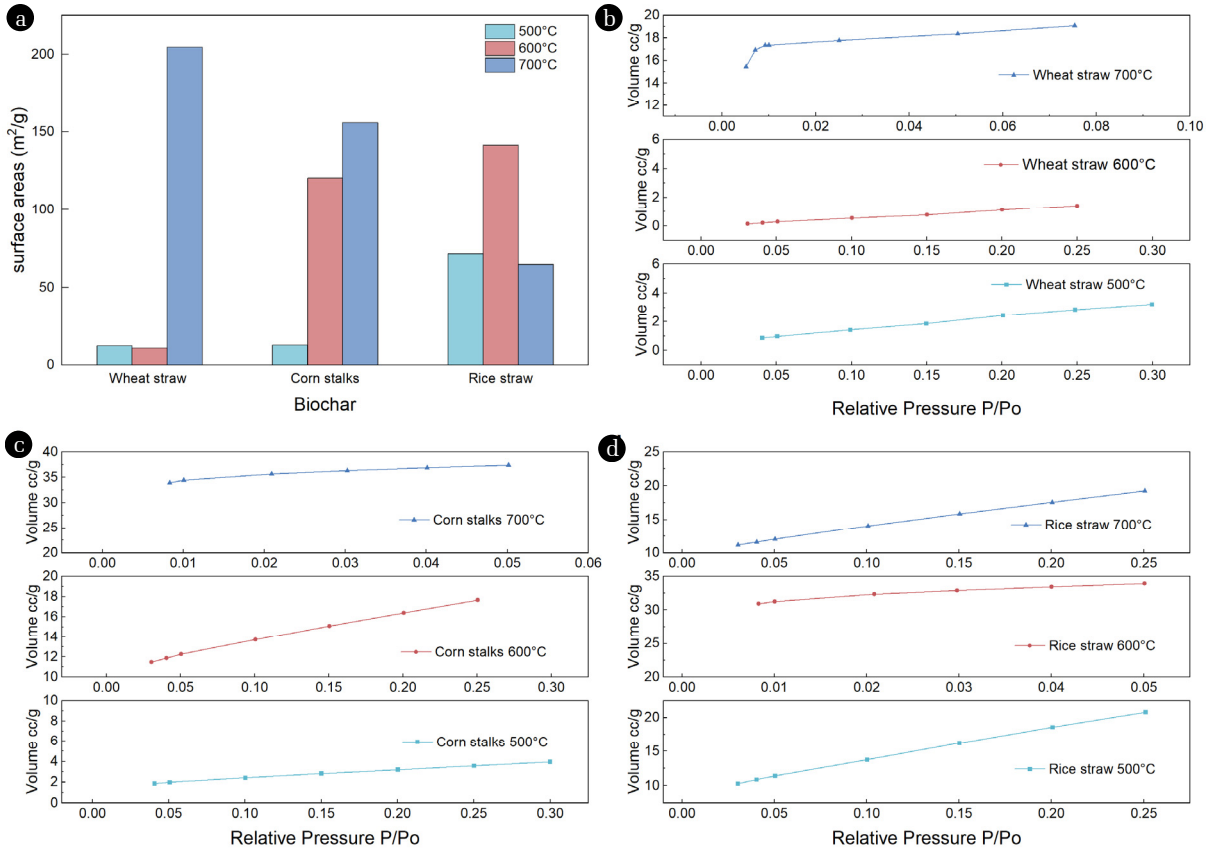

Fig. S1. (a) Specific surface areas of different BC; Adsorption isotherms of different BC: (b) Wheat straw, (c) Corn stalks, (d) Rice straw.

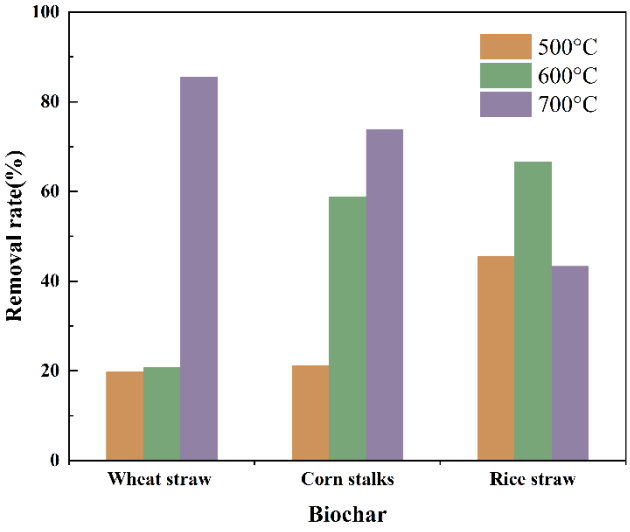

Fig. S2. Congo red adsorption of different BC (mBC=0.4 g, CCR 250 mg/l, t:24h).

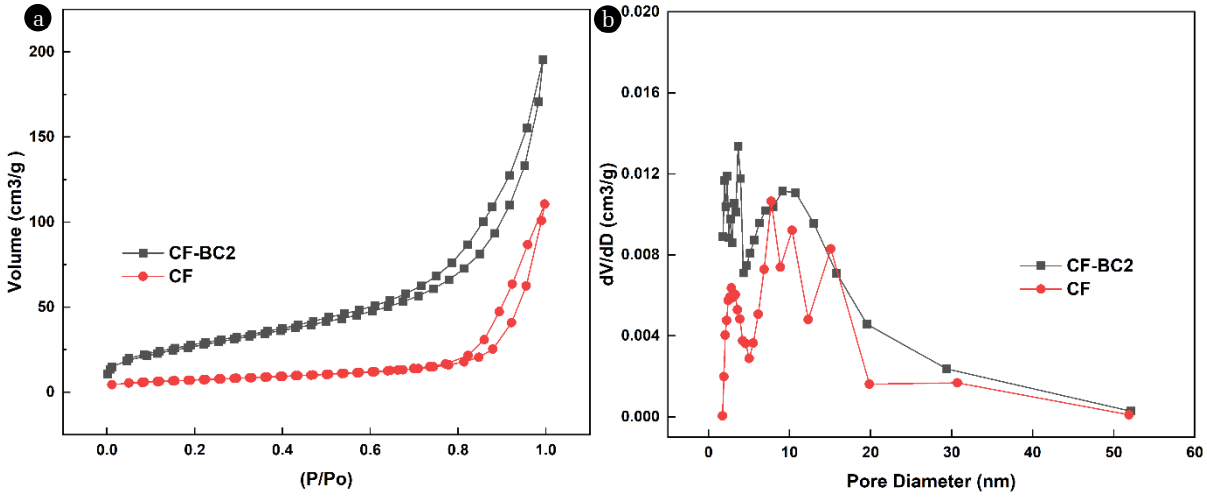

Fig. S3. The nitrogen adsorption-desorption isotherms and (b) pore size distribution of CF and CF-BC2 composite.

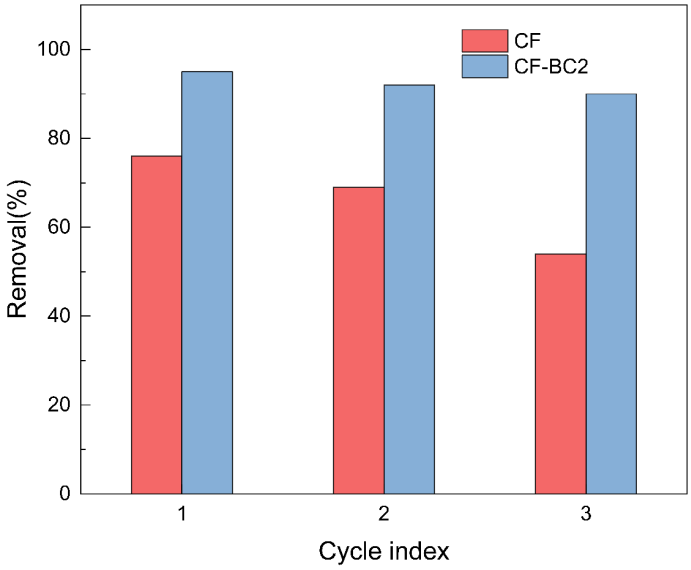

Fig. S4. Removal rates of CR by regenerated CF and CF-BC2.

Table S1. Elemental composition of BC

elements	C	O	Si	K	Ca	Mg	Cl	Al
Concents(%)	35.34	31.92	15.45	5.67	3.16	0.8	1.15	1.29

Table S2. Contents of C, O, Fe and Cr elements in CF-BC composite

Concents	**C**	**O**	**Fe**	**Cr**
CF-BC1	3.85%	12.15%	75.25%	6.19%
CF-BC2	9.17%	17.41%	64.21%	5.34%
CF-BC3	6.25%	13.28%	70.01%	5.57%

Table S3. The concentration of metal ions in the supernatant after adsorption reaction at pH=2

category	**Fe（mg/L）**	**Cr（mg/L）**
Leaching concentration	UD	4.81
EPA standard	/	5

Note: UD indicates no detection

Table S4. Langmuir and Freundlich isotherm constants for CR on CF

Temperature	Langmuir model			Freundlich model		
	Q_0 (mg/g)	K_L (L/mg)	R^2	K_F (mg/g)	n	R^2
25℃	305.8	0.0083	0.9758	21.1	2.49	0.9366
35℃	406.5	0.0145	0.9655	42.2	2.78	0.9649
45℃	438.6	0.0358	0.9867	53.2	2.57	0.7361

Table S5. Langmuir and Freundlich isotherm constants for CR on CF-BC2

Temperature	Langmuir model			Freundlich model		
	Q (mg/g)	K_L (L/mg)	R^2	K_F (mg/g)	n	R^2
25℃	526.3	0.0131	0.9543	34.0	2.26	0.9849
35℃	675.7	0.0134	0.9774	29.9	1.84	0.9823
45℃	819.7	0.0179	0.8738	37.8	1.72	0.9894

Table S6. Comparison of various adsorbent recycling.

absorbent	dyes	cycle efficiency/times	reference
Fe@graphite	Basic Red 46	91.7%/3	[1]
Bi2O3@GO	Rhodamine-B	80.1%/7	[2]
ELM	Methylene blue	90%/7	[3]
MCDs	Food Yellow 3	85%/5	[4]
Fe3O4/C-ACLS	Congo red	87%/5	[5]
ZAS/GRM	Congo red	88.7%/3	[6]
CAC-850–2	Congo red	82.09%/5	[7]
CF-BC	Congo red	90%/3	This Paper

References

1. Konicki W, Hełminiak A, Arabczyk W et al. Adsorption of cationic dyes onto Fe@graphite core–shell magnetic nanocomposite: Equilibrium, kinetics and thermodynamics. *Chem. Eng. Res. Des.* 2018;129:259–270. https://doi.org/10.1016/j.cherd.2017.11.004.
2. Das TR, Patra S, Madhuri R et al. Bismuth oxide decorated graphene oxide nanocomposites synthesized via sonochemical assisted hydrothermal method for adsorption of cationic organic dye. *J. Colloid. Interface. Sci.* 2018;509:82–93. https://doi.org/10.1016/j.jcis.2017.08.102.
3. Zereshki S, Daraei P, Shokri A. Application of edible paraffin oil for cationic dye removal from water using emulsion liquid membrane. *J. Hazard. Mater.* 2018;356:1–8. https://doi.org/10.1016/j.jhazmat.2018.05.037.
4. Zheng C, Zheng H, Wang Y, Liu, Liu S. Modified magnetic chitosan microparticles as novel superior adsorbents with huge “force field” for capturing food dyes. *J. Hazard. Mater.* 2019;367:492–503. https://doi.org/10.1016/j.jhazmat.2018.12.120.
5. Jiang C, Wang X, Qin D et al. Construction of magnetic lignin-based adsorbent and its adsorption properties for dyes. *J. Hazard. Mater.* 2019;369:50–61. https://doi.org/10.1016/j.jhazmat.2019.02.021.
6. An D, Sun Y, Yang YL et al. A strategy-purifying wastewater with waste materials: Zn2+ modified waste red mud as recoverable adsorbents with an enhanced removal capacity of Congo red. *J. Colloid. Interface. Sci.* 2023;645:694–704. https://doi.org/10.1016/j.jcis.2023.04.176.
7. Wang Q, Luo C, Lai Z et al. Honeycomb-like cork activated carbon with ultra-high adsorption capacity for anionic, cationic and mixed dye: Preparation, performance and mechanism. *Bioresour. Technol.* 2022;357:127363. https://doi.org/10.1016/j.biortech.2022.127363.